RESEARCH PAPER

Structural, Morphological and Anti-Bacterial Analysis of Nanohydroxyapatite Derived from Biogenic (SHELL) and Chemical Source: Formation of Apatite

Chimmachandiran Suresh Kumar[1,2], Kaliyan Dhanaraj[3], Ramasamy Mariappan Vimalathithan[4], Perumal Ilaiyaraja[5] and Govindhasamy Suresh[6*]

** gsureshphy_1983@yahoo.com*

Received: September 2020 Revised: November 2020 Accepted: December 2020

[1] Research and Development Centre, Bharathiar University, Coimbatore, Tamilnadu, India
[2] Department of Physics, Thiruvalluvar College of Engineering and Technology, Vandavasi, Tamilnadu, India
[3] Department of Physics, Arunai Engineering College, Tiruvannamalai, Tamilnadu, India
[4] Department of Physics, Salem Sowdeswari College (Govt. Aided), Salem, Tamilnadu, India
[5] Chemistry Divisions, School of Advanced Sciences, Vellore Institute of Technology Chennai campus, VIT University, Chennai, Tamilnadu, India
[6] Department of Physics, Aarupadai Veedu Institute of Technology, Vinayaka Mission's Research Foundation, Chennai - 603 104, Tamilnadu, India

DOI: 10.22068/ijmse.18.1.10

Abstract: *The Nano Hydroxyapatite (HAp), HAp/PEG and HAp/PVP powders derived from both Gastropod shell (natural source) and chemical precursor by the precipitation method were characterized through various characterization techniques such as FT-IR, XRD, SEM-EDX, TEM, Antibacterial activity and SBF analysis. Based on the structural, chemical, morphological and biological characteristics, HAp/PVP from natural and chemical precursors have been compared. Calculated structural parameters, crystallinity index, C/P ratio, morphology, antibacterial activity and SBF analysis of the products show that HAp/PVP-S (derived from a natural source) exhibits good mechanical property, rod like morphology, good antibacterial activity and apatite formation ability after 14 days. EDX analysis also shows the presence of carbon and sodium in HAp/PVP-S. Comparative analysis reveals that characteristics of HAp/PVP-S such as high carbonate content, low crystallite size, poor crystalline nature, presence of trace metal, non-stoichiometric elemental composition and rod like crystals which are matched with the characteristics of biological apatite. Thus, the HAp/PVP-S has the ability to form bone apatite.*

Keywords: *Hydroxyapatite, Precipitation Method, Comparative Analysis, Antibacterial Activity, SBF Analysis.*

1. INTRODUCTION

Bone is a living connective tissue that provides structural support to body organs and is basically composed of an organic phase (20-30 wt %), inorganic phase (60-70 wt %) and water (around 5 wt %) [1]. The organic phase provides elasticity, flexibility and resistance to the bone. In the inorganic matrix, Hydroxyapatite (HAp; $Ca_{10}(PO_4)_6(OH)_2$) is the main component and is a well-known biomaterial due to its significant biocompatibility, bioactivity, and thermodynamic stability in bones [2]. Ions such as carbonate, magnesium, fluoride and sodium are the minor components of the inorganic matrix; the whole matrix gives hardness and stiffness to the bone [1]. Of these, carbonate (CO_3^{2-}) is the most abundant with 2.3 - 8 wt%. The CO_3^{2-} ions may either occupy in the OH^- sites (A-type HAp), PO_4^{3-} sites (B-type HAp), and occupy in both OH^- and PO_4^{3-} sites (AB-type HAp) [3]. The above mentioned substitution makes a decrease in crystalline size and crystalline nature, change in lattice dimensions, and increase in disorder and solubility in the apatite structure [4]. These parameters are essential to improve bioactivity and bone apposition [5].

Nanostructured HAp promotes osteoblast adhesion, proliferation, osseointegration, implant–cell interaction, bone growth, dissolution rate and new bone growth [6]. Generally, HAp does not have all necessary mechanical properties including the capacity to bear a high load for above said applications and thus polymers are added to HAp for improving the mechanical stability and biological properties [7]. To control the nucleation and crystal growth of HAp, water soluble PVP is used as a capping agent [8]. PEG is another most promising polymer in biomedical research and applications including bone tissue

[DOI: 10.22068/ijmse.18.1.10]

engineering [9] due to its excellent biocompatibility and biodegradable nature [10].
Interestingly, HAp from natural sources has some trace elements such as carbonate, sodium, magnesium, iron, etc. as in the natural bone [1]. These elements play an important role in the regeneration of bones, osteointegration process and other applications [11, 12]. Also, extraction from natural sources can be considered to be an environmentally friendly, sustainable and economical process [11]. To ensure the presence of required qualities of HAp derived from natural sources, a detailed comparative study is needed to be carried out between the HAp extracted from natural and chemical source.
In the recent past, some comparative studies have been carried out in HAp in possible manners and inferences are as follows. Comparative crystallographic analysis of HAp derived from the chemical route, coral and xenogeneic bone shows that the properties and phase purity depend on preparation method and source, and carbonate ions were observed in the HAp derived from natural bones [13]. Swain and Sarkar [14] made a comparative study between the Hydroxyapatite spherical nanopowders and elongated nanorods. The spherical powder has a tendency to form a carbonated HAp phase [14]. HAp had been prepared from natural bones (human, bovine, camel and horse bones), and chemical source via the sol-gel method by Rahavi [15]. They found that HAp derived from a natural source has required physicochemical property and most importantly stimulated cell proliferation (no cytotoxicity) compared to the samples prepared using chemical precursors. A thorough comparative analysis was carried out between the characteristics of HAp synthesized through sol–gel and wet chemical precipitation methods by Ramesh et al. [16]. In this analysis, similar suitable characteristics to natural bone such as smaller crystallite size, poor crystalline nature, high surface activity and nanoscale needle-like structures were achieved in the wet chemical precipitated HAp. Recently, both Mondal et al. [6] and Sossa et al. [17] have executed different comparative studies between the natural sources (fish/porcine bone) and chemical source derived HAps. The non-stoichiometric nature, non-toxic behavior, good SBF interactions, enhanced cellular attachment and proliferation are achieved in the HAp derived from natural sources. Characteristics of

HAp derived from bovine bones and obtained through the wet chemical precipitation method were compared and attained the above said suitable characteristics in the bovine bone derived HAp [18]. Characteristics of nano-crystalline HAp derived from Mercenaria clam shells were compared with phosphoric acid derived HAp by Pal et al. [19], here also, non-toxic nature with respect to fibroblast and osteoblast-like cells achieved in Clam shell derived HAp. Lee et al. [20] compared the HAp derived from both sea and egg shell. They got some useful presences such as sodium, strontium and carbonate along with HAp in sea shell derived HAp. Based on the source and processing methods, properties of HAp such as Ca/P ratio, particle size, morphology, carbonate content, crystallinity and phase assemblage could be varied and important properties of bone apatite could also be presented in the natural source [11]. Though there are many comparative reports available for HAp, it is scanty for polymers assisted HAp. Thus, the present study has indented to compare the characteristics of polymer assisted HAp derived from Vokesimurex elenensis shell (natural source) (HAp-S) and chemical source (HAp-C). The Vokesimurex elenensis is well known recognized abundant shell (length: 120 mm) and are composed of >95–99.9% $CaCO_3$**.** Up to 60% of the product by weight is largely considered as waste and end up in land□ll [23]. As a consequence, it is essential to get HAp from Vokesimurex elenensis shell.
The present study is aimed to (i) prepare polymers (PEG and PVP) assisted HAp-S and HAp-C by simple precipitation method (Practical advantages: low energy consumption, high yield and purity, nanophase particle size control, simple experimental stages, large scale production, homogenous mixing and a meager amount of harmless by-products) [18, 21]; (ii) characterize the products by FT-IR, XRD, SEM-EDX, TEM-SAED, Antibacterial activity and SBF analyses; (iii) calculate the crystallite size, crystanality index, C/P ratio and structural parameters for all the products using FT-IR and XRD, and (iv) assess the best product from each source and compare their characteristics based on the obtained functional, structural, chemical,

[DOI: 10.22068/ijmse.18.1.10]

morphological and biological characteristics.

2. EXPERIMENTAL PROCEDURE

2.1. Materials

The shells of Vokesimurex elenensis (Class: Gastropoda; Phylum: Mollusca) were collected from various sites of Vellar Estuary situated at Parangipet, Tamilnadu, India (Lat: 11º20' 25.55"N, Long: 79º45' 38.62"E) and other significance of the sampling site was reported in our previous article [22]. The obtained shells were washed in running water for several times. To remove the meat and algae content the shells were soaked in hot water for 30 min. Finally, washed with distilled water and then dried it for 3 hrs at 100 ºC in a hot air oven.

The starting materials were Nitric acid (HNO_3), Diammonium hydrogen phosphate ($(NH_4)_2\ HPO_4$), Calcium nitrate tetrahydrate (Ca $(NO_3)_2\ 4H_2O$), Sodium hydroxide (NaOH), Polyvinylpyrrolidone (PVP, Mw: 40000), Polyethylene glycol (PEG, Mw: 6000), Acetone and Deionized water. All the chemicals were analytical reagent grades with 99% purity and purchased from Merck.

2.2. Synthesis of Hydroxyapatite from Vokesimurex Elenensis Shell (HAp-S)

The HAp was prepared through the precipitation technique by using CaO derived from dried shells as per the procedure reported by Dhanaraj and Suresh [22]. 0.1 M of Ca $(NO_3)_2$ solution was prepared by dissolving the CaO into concentrated HNO_3 (25 % of Nitric acid) and diluted with deionized water. 0.06 M of $(NH_4)_2\ HPO_4$ solution was slowly added into the 0.1 M of Ca $(NO_3)_2$ (obtained amount of Ca/P ratio was 1.67) and the pH of the reaction medium was maintained as 9 by using 1M NaOH solution. The obtained precipitate was centrifuged for 15 hrs and washed with deionized water. Then, the precipitate was filtered and dried in a hot air oven for 3 hrs at 100 ºC. Finally, the obtained powder was calcined at 900 ºC for 3 hrs to get HAp. The possible chemical reactions are given below:

$$CaO + 2HNO_3 \rightarrow Ca\ (NO_3)_2 + H_2O \quad \uparrow \qquad (1)$$

$$10\ Ca\ (NO_3)_2 + 6\ (NH_4)_2\ HPO_4 \rightarrow Ca_{10}\ (PO_4)_6\ (OH_2) + 6\ NH_4\ NO_3 \qquad (2)$$

$$(PO_4)_6(OH_2) + 6NH_4NO_3 \xrightarrow[900\ ºC/3hs]{\Delta} Ca_{10}(PO_4)_6(OH_2) \qquad (3)$$

(Hydroxyapatite)

2.3. Synthesis of PEG and PVP Assisted HAp-S

PEG (1 mM in 25 mL of deionized water) was added drop by drop to the pure HAp under continuous stirring. The obtained precipitate was washed several times using deionized water, dried (100 °C for 3 hrs) and calcined (900 °C) to obtain HAp/PEG. The same procedure was repeated to obtain the HAp/PVP.

2.4. Synthesis of Hydroxyapatite from Chemical Source (HAp-C)

Instead of calcium oxide (CaO), 0.1 M of commercially available calcium nitrate tetrahydrate (Ca $(NO_3)_2\ .4H_2O$) was taken as a calcium source. All other materials and procedure were similar to the preparation of HAp from the shell.

Samples prepared from the shell (natural source) are represented as HAp-S, HAp/PEG-S and HAp/PVP-S, similarly chemically derived samples are represented as HAp-C, HAp/PEG-C and HAp/PVP-C.

2.5. Antibacterial activity test

The in vitro antibacterial activity of HAp, HAp/PEG and HAp/PVP derived from both sources have been studied against Escherichia coli and Staphylococcus aureus by the agar well diffusion method as reported in Dhanaraj and Suresh [22]. Negative control as well as calcined samples of HAp, HAp/PEG and HAp/PVP were loaded on marked wells with the help of micropipette and plates, and incubated for 24 hrs at 37 °C. The zone of growth inhibition was measured using HiAntibiotic Zonescale in Himedia and expressed in mm. All experiments were performed in triplicate under aseptic conditions.

2.6. SBF Analysis

The bioactivity of the prepared samples was studied using simulated body fluid (SBF). The solution was prepared by dissolving appropriate quantities of chemicals in distilled water and reagents were added one by one in 1000 ml of water as per the procedure given by Tank et al. [24]. The prepared sample was soaked in SBF solution for various days such as 3, 7

[DOI: 10.22068/ijmse.18.1.10]

and 14 days at 37 ± 0.5ºC.

3. RESULTS AND DISCUSSION

3.1. FT-IR Spectroscopic Analysis

FTIR spectra of the HAp-S, HAp/PEG-S and HAp/PVP-S are shown in Figure 1 (a, b and c), respectively. FTIR spectrum of HAp-S (Figure 1a) shows the absorption peaks at 3646 & 3574 (stretching vibration of OH^-), 2520 (adsorbed water), 1996 (PO_4^{3-}), 1460 and 1412 (ν_3, asymmetric stretching of carbonate), 1093 & 1049 (ν_3: stretching vibration of the O-P-O), 961 (ν_1: stretching vibration of the O-P-O), 877 (ν_2, out of plane bend of carbonate), 712 (formation of $CaCO_3$), 632 (libration mode of OH^-), 602 & 567 (ν_4 : triply degenerated bending mode of the O-P-O), and 474 (ν_2 : asymmetric stretching vibration mode) cm^{-1} [6, 25]. These observations demonstrate the presence of HAp in the samples. Additionally, three medium peaks at 877, 1412 and 1460 cm^{-1} show B-type HAp [26]. Similar observations were reported in the literature [26-30]. When adding the PEG (Figure 1b), the above said characteristics vibration modes of phosphate, hydroxyl and carbonate are observed with slight deviations. Intensities of CO_3^{2-} peaks are high. The intensity and broadness of the ν_4 (602 and 567 cm^{-1}) doublet are decreased. A weak peak at 634 cm^{-1} is almost disappeared and a new minor peak at 712 cm^{-1} appears. The presence of minor peak at 712 cm^{-1} is due to the formation of $CaCO_3$. Due to the reaction of CaO and CO_2, a small amount of $CaCO_3$ is obtained in the CO_2 rich atmosphere [31]. Some literature [29, 31] had reported the same information about this peak in the HAp. The presence of amide is also assessed by a small minor peak at 1794 cm^{-1} [22].

All the characteristics vibrational modes of phosphate, carbonate and hydroxyl bands are presented with slight deviations in HAp/PVP-S (Figure 1c). When compared with Figure 1(b), intensity of ν_4 doublet (603 and 569 cm^{-1}) is decreased. The existence of CO_3^{2-} in the samples could be due to the chemisorptions of atmospheric CO_2 on the surface of HAp under alkaline pH [32]. The presence of well-defined carbonate strong doublet (ν_3) at 1412 and 1461 cm^{-1}, and intense ν_2 at 875 cm^{-1} indicates the strong substitution of carbonate in HAp while adding PVP due to the better encapsulation of the polymer on the product. In both HAp/PEG-S and HAp/PVP-S, as polymers adhere to the surface of particles, high carbonate content is possible [33].

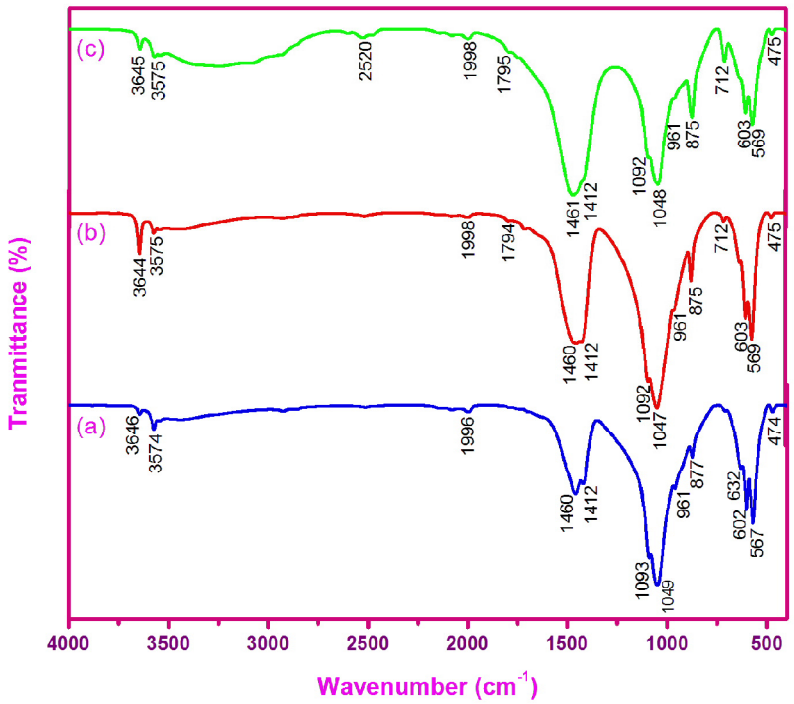

[DOI: 10.22068/ijmse.18.1.10]

Fig. 1. FTIR spectra of the HAp-S (a), HAp/PEG-S (b) and HAp/PVP-S (c) at 900 ºC.

Figure 2 (a, b and c) shows the FTIR spectra of HAp-C, HAp/PEG-C and HAp/PVP-C, respectively. FTIR spectrum of HAp-C (Figure 3a) shows the absorption peaks at 3575, 1996, 1456, 1091, 1048, 961, 875, 632, 604, 569 and 476 cm^{-1}. Based on the above assignments, the formation of HAp is assessed. When adding the polymers (PEG and PVP), intensities of carbonate and hydroxyl peaks are faintly increased, and the phosphate peak is faintly decreased.

A high degree of crystallinity of the HAp could be assessed by sharp and splitting peaks at 565/605 and 1055/1100 cm^{-1} [26]. In the naturally derived products of the present case, intensities of the above said splitting are decreased in HAp/PEG-S and still decreases (Figure 1) in HAp/PVP-S. This dictates that HAp-S has a high degree of crystallinity; it is decreases for HAp/PEG-S and further decreases for HAp/PVP-S. In the case of chemically derived products, there is no noticeable change and many variations in crystallinity are observed. These observations are confirmed in the Crystallinity Index calculations (Table 1).

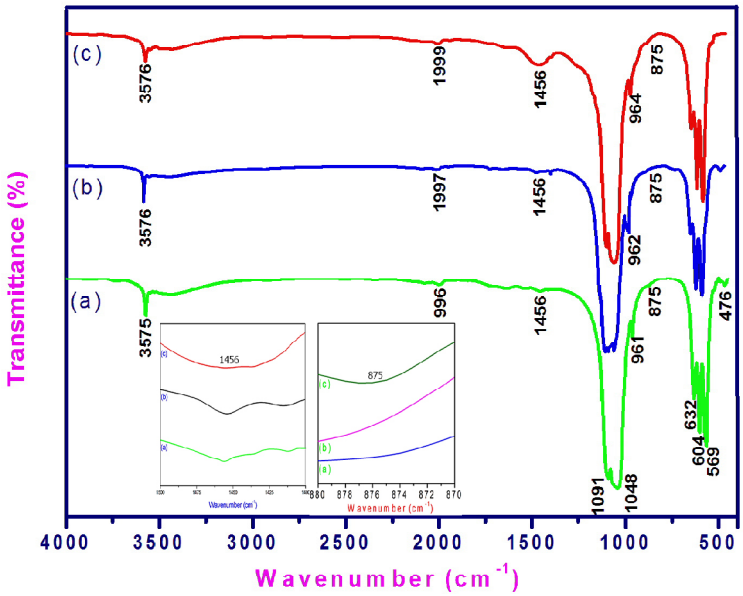

Fig. 2. FTIR spectra of the HAp-C (a), HAp/PEG-C (b) and HAp/PVP-C (c) at 900 ºC. Inset shows magnified image of peaks at 875 and 1456 cm^{-1}.

Table 1. Structural parameters, Crystallinity Index and C/P ratio of HAp, HAp/PEG and HAp/PVP derived from both Natural and chemical sources

Sample ID	Lattice parameters			Volume of Unit cell V (A°)	Average crystallite size D (nm)	Average microstrain (ε) x 10^{-3}	Average dislocation density (δ) x 10^{14}	Average stacking fault (SF) x 10^{-2}	CI (FTIR)	CI (XRD)	C/P
	a = b (A°)	c (A°)	c/a								
HAp - S	9.3689	6.8835	0.7347	523.27	68.0337	0.512	2.2617	0.177	4.623	1.8449	0.296
HAp/PEG - S	9.3346	6.8837	0.7374	519.41	56.3941	0.647	3.7490	0.223	4.334	1.3033	0.312
HAp/PVP - S	9.3035	6.8839	0.7399	516.02	44.9871	0.818	6.0851	0.283	4.134	1.2821	0.356
HAp - C	9.3887	6.8832	0.7331	525.44	78.5327	0.444	1.6214	0.1552	7.365	1.6011	0.058
HAp/PEG - C	9.3444	6.8833	0.7366	520.51	56.4680	0.614	3.2469	0.2126	7.1323	1.6174	0.093
HAp/PVP - C	9.3208	6.8835	0.7385	517.90	51.2103	0.682	4.0372	0.2362	6.9876	1.5735	0.163

[DOI: 10.22068/ijmse.18.1.10]

3.1.1. Crystallinity Index (CI)

The crystallinity index (CI) represents a measure of the perfection and degree of ordering in a sample. It is known that the high and low CI values are connected with more ordered and poorly crystallized crystals respectively [34, 35]. It is negatively related to HAp crystal size and has apparent influences on the hardness and density of the material [34, 36, 37]. CI is calculated (Table 1) from both FTIR (height method) and XRD (method and formulae) used by the other researchers [35, 36, 38, 39]. Both methods should be considered qualitatively complementary and not quantitatively the same [36].

In the natural source, both CI values are high for HAp-S, values are decreased for HAp/ PEG-S and low for HAp/ PVP-S (Table 1). This dictates that degree of crystallinity is high, moderate and poor for HAp-S, HAp/PEG-S and HAp/PVP-S, respectively, as observed earlier. A decrease in the crystallinity in polymer composite could be due to the utilization of the part of external energy for ordering the atoms, remaining part of the external energy is utilized for decomposing polymers [40]. In the case of chemical source, no much change is observed in CI values while adding the polymers. High substitution of CO_3^{2-} in HAp/PVP-S reduces its crystallinity considerably; this substitution is low in HAp/PVP-C [40]. HAp with reduced crystallinity has high solubility and protein absorption capacity [37].

3.1.2. Carbonate to Phosphate (C/P) Ratio

In order to assess the carbonate incorporation (amount of carbonate) into the hydroxyapatite lattice, carbonate to phosphate (C/P) ratio is need to calculate (Table 1) by dividing the intensity of absorption peak at 1460 cm^{1} (amount of carbonate) by 1049 cm^{-1} (amount of phosphate) [35, 41]. In natural source, C/P value is low for HAp-S (0.296), value is increased for HAp/PEG-S (0.312) and high for HAp/PVP-S (0.356). In the case of chemical source, the absorption peak at 1446 cm^{-1} is taken, values are smaller and the above same increasing trend is observed. This indicates that in both sources, the amount of carbonate content is high in HAp/PVP, decreased in HAp/PEG and low in HAp as already discussed.

3.2. XRD Analysis

X-ray diffraction patterns of HAp-S, HAp/PEG-S and HAp/PVP-S are shown in Figure 3. Formation of hexagonal Hydroxyapatite crystalline phase (JCPDS#09-0432) [42] in HAp-S (Figure 3a) is assessed by the identified reflections such as (200), (111), (002), (210), (211), (112), (300), (202), (310), (311), (113), (203), (222), (312), (123), (321), (402), (004) and (322). In the HAp-C, identified reflections are almost the same (Figure 4a) which confirms the presence of above said hexagonal hydroxyapatite crystalline phase. While adding the PEG and PVP in HAp-S, diffraction peaks are broadened and intensities of peaks are decreased (Figures 3b and c). These variations are high for HAp/PVP-S due to the high carbonate substitutions, it is not visible in Figure 4. These infer that there is a change between the ratio of hexagonal lattice and primitive lattice [43], crystallite size and crystalline nature are decreased when adding the polymers. The intensity of carbonate peak (210) is high in HAp/PEG-S and increases in HAp/PVP-S which indicates the high presence of carbonate.

When adding the polymers mostly PVP in HAp derived from both sources, the intensity of (002) is increases and intensity is high in the HAp/PVP-S. This indicates that HAp/PVP-S particles exhibit a much higher tendency to grow along the c-axis [44] and growth in the c-axis is its inherent property which facilitates the formation of rods rather than particles [45] (confirmed by SEM and TEM analyses).

3.2.1. Calculation of Structural Parameters

CO_3^{2-} substitution affects HAp physical parameters (lattice constants, crystallite size, crystalline nature, microstrain, dislocation density and stacking fault) [41]. Hence, it is important to calculate the above said crystallographic structural parameters for the present samples (Table 1) based on the literature [36, 46]. Changes in the physical parameters influence the chemical reactivity, stability, opacity, efficacy of delivery, texture, flowability, packing density, viscosity, porosity and strength of materials [8].

For both sources, calculated lattice constants are well matched with the above said JCPDS (Table 1). While adding the polymers, values of lattice constants ‘a’ and ‘c’ are decreases and increases respectively. For HAp/PVP-S, low ‘a’ and high

[DOI: 10.22068/ijmse.18.1.10]

'c' values are observed (Table 1). Due to the carbonate incorporation in the lattice, 'a' axis is contracted and 'c' axis is expanded as shortening the bond length between the P atom at the tetrahedral site and the oxygen atoms on the mirror plane of the phosphate tetrahedron [40]. A decrease in crystallinity, a great increase of solubility in both in vitro and in vivo tests and higher affinity for the human trabecular osteoblastic cell can be possible due to the presence of type B-carbonate in the apatite lattice [47].

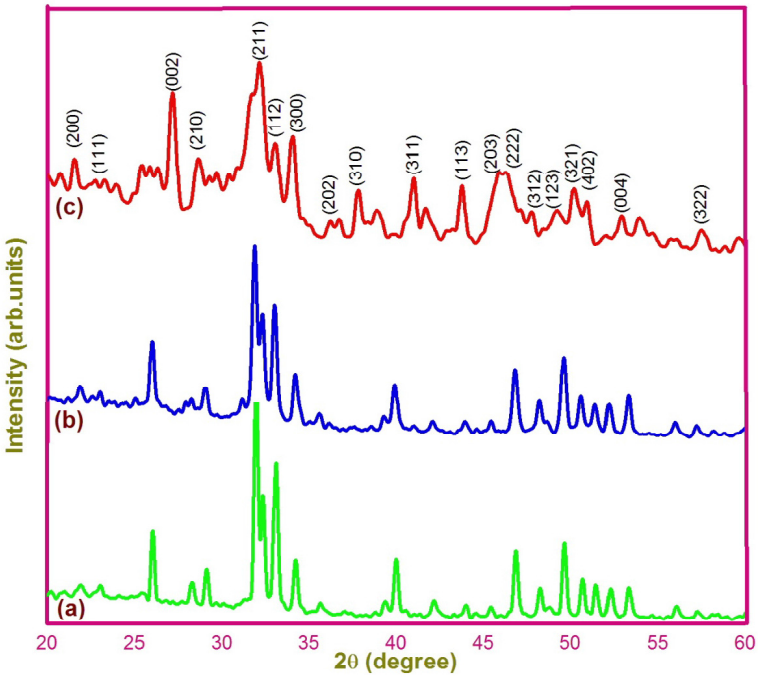

Fig. 3. XRD patterns of the HAp-S (a), HAp/PEG-S (b) and HAp/PVP-S (c) at 900 ºC.

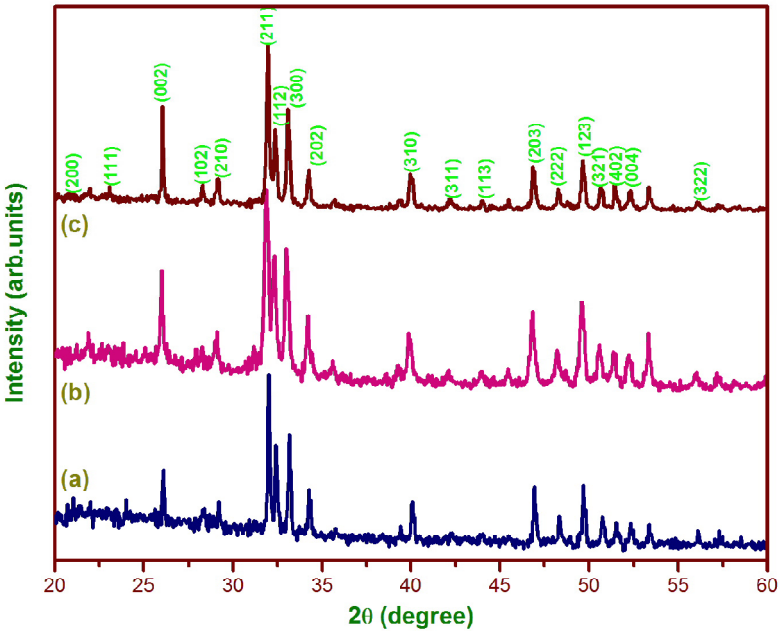

Fig. 4. XRD patterns of the HAp-C (a), HAp/PEG-C (b) and HAp/PVP-C (c) at 900 ºC.

[DOI: 10.22068/ijmse.18.1.10]

Table 1 shows the average crystallite sizes of HAp, HAp/PEG and HAp/PVP derived from both sources calculated by well known Debye-Scherrer formula [46, 48]. In both cases, calculated crystallite sizes are low for polymer assisted HAps and very low for HAp/PVP-S. Polymers can cover the larger surface area of the nanoparticles as they are good stabilizing agents. While adding PEG and PVP, it restricts the growth of the particle due to the higher additional steric hindrance [43]. Particularly, PVP stabilizes the nanoparticles through higher additional steric hindrance by coordination of C=O of the PVP molecule with Ca^{2+} in HAp [43] and more polar activity in PVP [33].

In both sources, values of microstrain, dislocation density and stacking fault are increased when adding the polymers (Table 1), especially HAp/PVP-S shows high values due to the high presence of CO_3^{2-} in the HAp structure which is the primary source of distortion of the crystalline network, creating micro-stresses and defects in its vicinity, greatly influencing its solubility [34]. As dislocation density, stacking fault and microstrain of the polymer assisted products are decreased, strength of products can be increased [49]. Table 1 shows that when the above said structural parameters (ε, δ and SF) are increases, crystallite size and nature decrease. Thus, HAp/PVP-S exhibits good mechanical property for bio-medical applications.

3.3. Morphological Analysis – SEM and TEM

SEM images of HAp-S, HAp/PEG-S and HAp/PVP-S (Figure 5a, b and c) show the mixed morphology, agglomerated particles and rod like structures, respectively. The TEM images (Figure 6a, b and c) of the products illustrate the particle, agglomerated majorly hexagonal and rod like structure respectively. Particles, agglomerated particles and hexagonal clusters are observed in HAp-C, HAp/PEG-C and HAp/PVP-C, respectively, through SEM images (Figure 5d, e and f). However, TEM images of the products show hexagonal particles, agglomerated particles and dense rod like structure in HAp, HAp/PEG and HAp/PVP (Figure 6d, e and f) respectively.

The formation of HAp nanoparticles could be explained through two steps (i) nucleation and growth to form HAp particles and (ii) the aggregation of elemental nanoparticles by molecular attractions of different nanometric/colloidal scale forces which cause surface free energy minimization. In both sources, when adding the PEG, the formation of agglomerated particles could be elucidated through further crystal growth at a constant residual super-saturation. Here PEG acts as a cementing agent between the aggregates to form agglomerate due to Van der Waals attraction [15]. According to Yelten and Yilmaz [18], agglomerates with different sizes in the structure were expected cases since the wet chemical precipitation technique relies on the nucleation-aggregation-agglomeration-growth mechanism. The surface-dominated properties of nanoparticles cause the particles to clump together which could be a possible reason for the agglomerate behavior which finds many applications, including drug delivery [17].

Usually, polymers have the strong ability to interact with nanoparticles through their coordination bonds or strong interactions of the functional head groups and thus kinetically control the growth rates of various faces of crystals, which could control the morphology. The PEG [HO–(CH_2–CH_2–O)n–H] is a linear and non-ionic long chain polymer with hydrophilic –O– and hydrophobic –CH_2–CH_2– radicals. Atom oxygen with more coordination abilities and negative charges in PEG can bind more strongly with positively charged HAp ions due to the electrostatic forces of attraction [50]. Thus, PEG inhibits the reactivities of HAp, slow down the growth and confined the hexagonal morphology through the degree of adsorption, the electrostatic force of attraction and interaction between the PEG molecules and Ca^{2+} ionic group [51].

In both sources, when adding PVP on HAp, the nanoparticles are formed as nanorods with defined boundaries (Figure 6c and f). PVP confines growth along with the side faces and activates growth along the end direction (c-axis), resulting in HAp nanorods [52]. Here, a large driving force is acted to maximize the contact area and minimize the surface energy.

As in the case of the biomineralization process, here also similar effects to result in the rod- like morphology. Two effects such as (i) spatial effect

[DOI: 10.22068/ijmse.18.1.10]

and (ii) electrostatic and hydrogen bond effects, are important roles of PVP. The hydrogen bond is formed between PVP and HAp through the abundant O–H groups located on the surface of HAp, which prevents the aggregation of the nanorods and the growth along the direction vertical to the c-axis [53]. Ostwald ripening and oriented attachment are two common mechanisms to understand the present crystal growth [53]. In the present case, the formation process of rod like HAp includes nucleation, growth, surface-regulating, Ostwald ripening and oriented attachment. This is the possible mechanisms for HAp nanorod [8, 52-54].

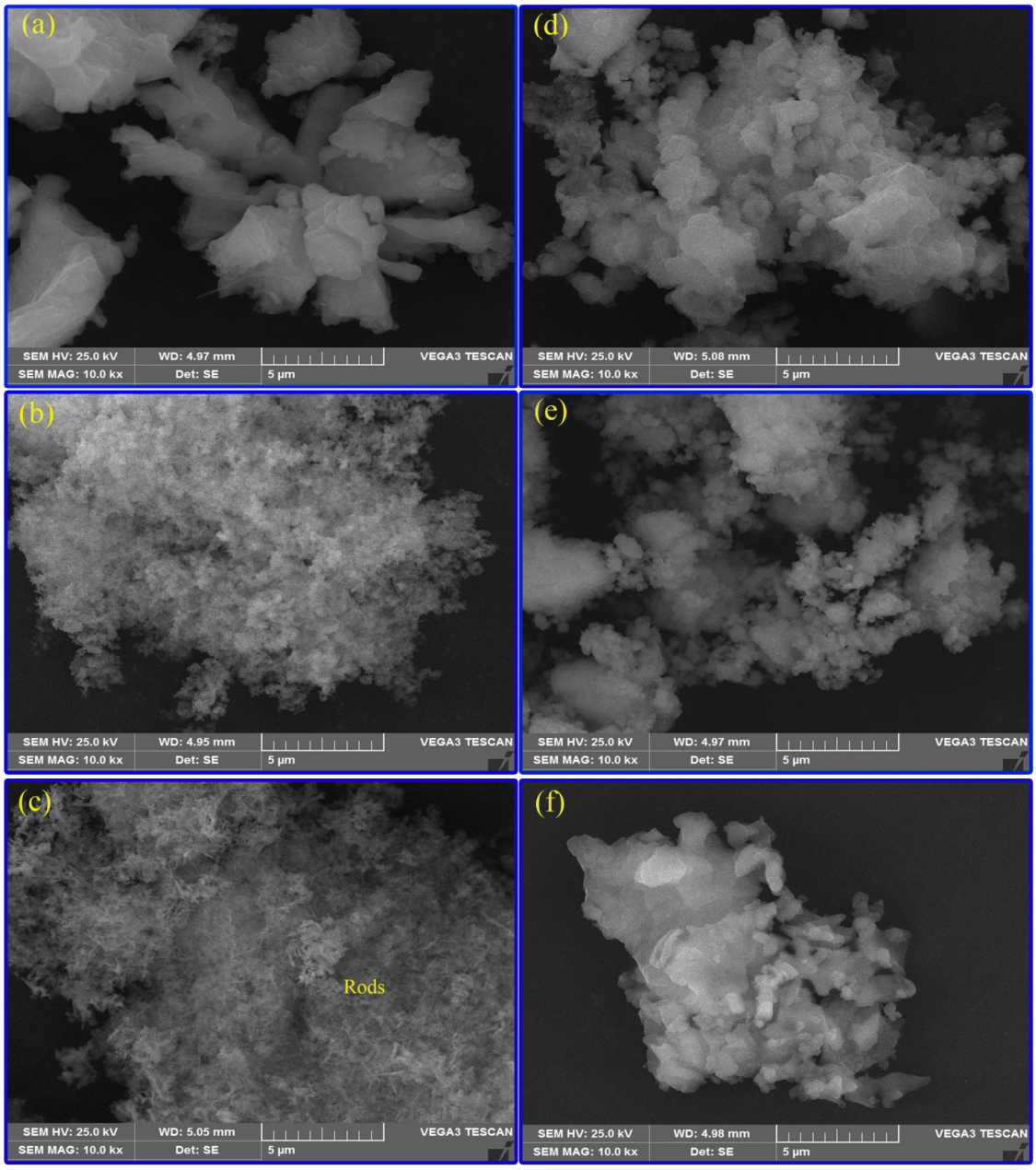

Fig. 5. SEM images of HAp-S (a), HAp/PEG-S (b), HAp/PVP-S (c), HAp-C (d), HAp/PEG-C (e) and HAp/PVP-C (f).

[DOI: 10.22068/ijmse.18.1.10]

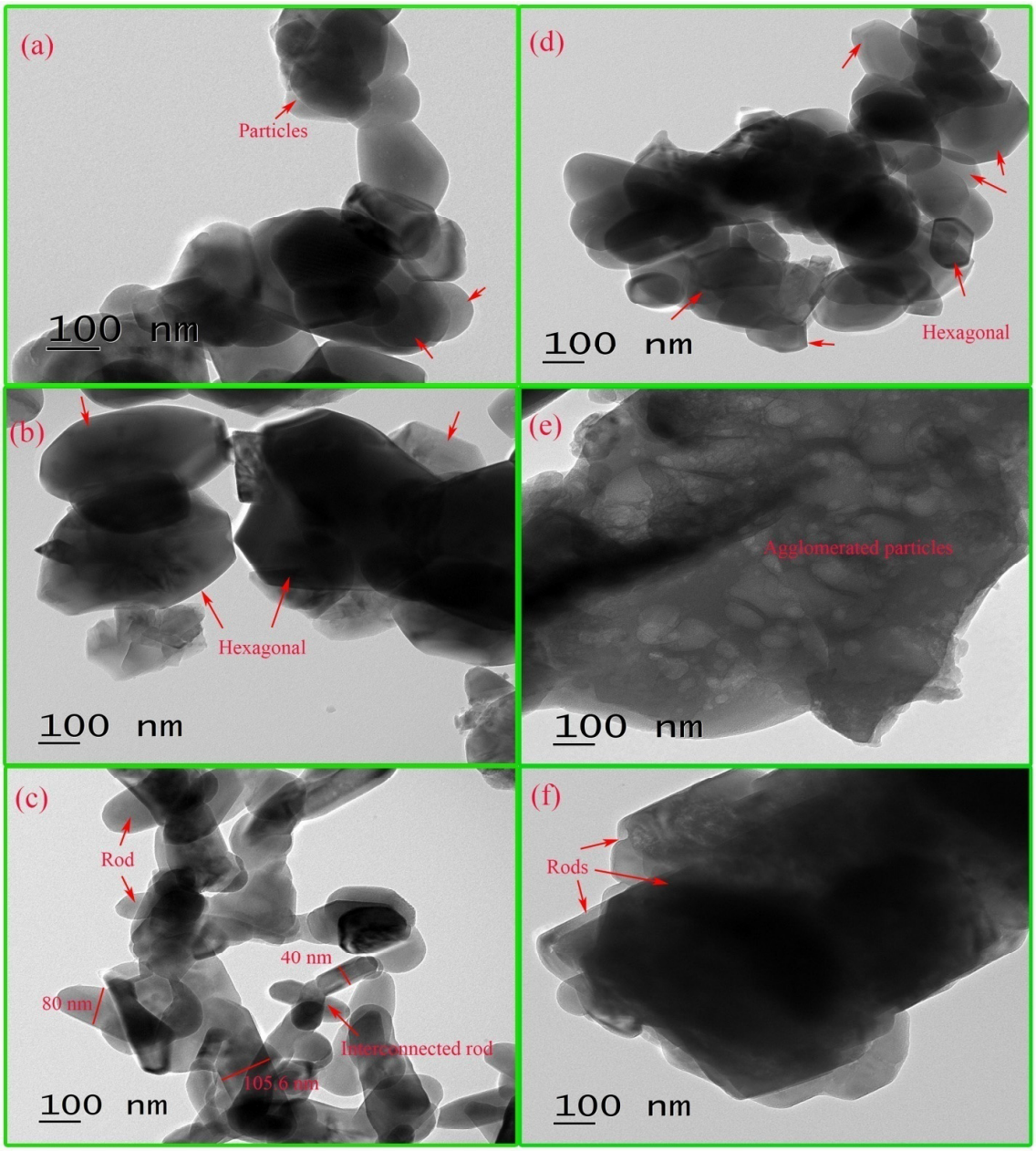

Fig. 6. TEM images of HAp-S (a), HAp/PEG-S (b), HAp/PVP-S (c), HAp-C (d), HAp/PEG-C (e) and HAp/PVP-C (f).

3.4. Elemental Composition -EDX

The EDX spectra of the HAp and HAp/PVP derived from shell source (Figure 7) show the presence of elements such as Ca, P, C, Na and O. However, elements such as Ca, P and O are only presented in HAp-C and HAp/PVP-C. The calculated Ca/P ratios of HAp/PVP-S and HAp/PVP-C are 1.76 and 1.68, respectively (Table 2). More deviation of Ca/P ratio in the HAp/PVP from the theoretical ratio also indicates the high substitution of carbonate and the presence of sodium in the lattice. The presence of sodium could enhance the B-type carbonate substitution in the lattice [55].

3.5. Antibacterial Activity

Figure 8 shows the antibacterial activities (zone of inhibition) of the HAp, HAp/PEG and HAp/PVP derived from both natural (a and b) and chemical

[DOI: 10.22068/ijmse.18.1.10]

source (c and d) against the E. coli and S. aureus. From the figure, all the products have moderate antibacterial activity. When adding the PEG and PVP, the zone of inhibition is increased in both sources and the highest zone of inhibition is attained in HAp/PVP-S (Figure 9). In both sources, it is found that the HAp/PVP has good sensible antibacterial activity against the E. coli and S. aureus. Recently, Metha and Kaith [56], reported about the sensible antibacterial property of HAp against the same bacterial strains and got comparable zone of inhibition values.

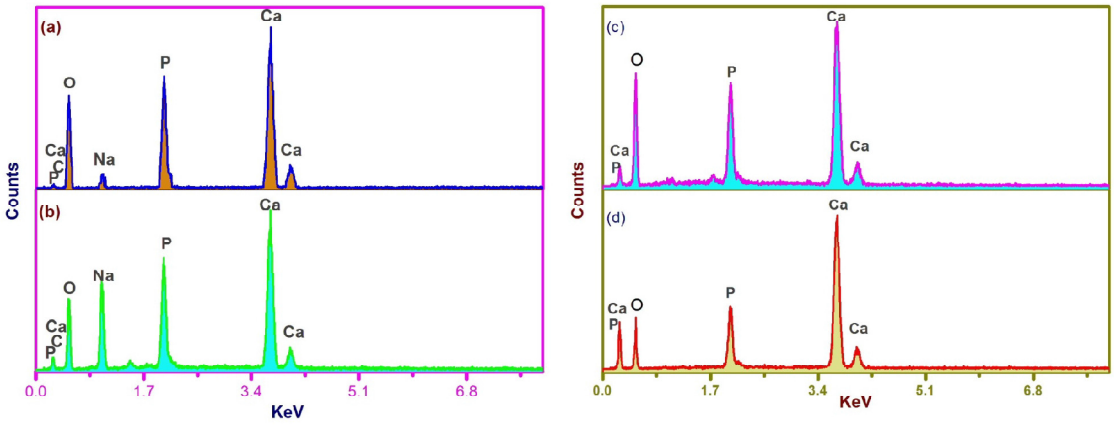

Fig. 7. EDX spectra of HAp-S (a), HAp/PVP-S (b), HAp-C (c) and HAp/PVP-C (d)

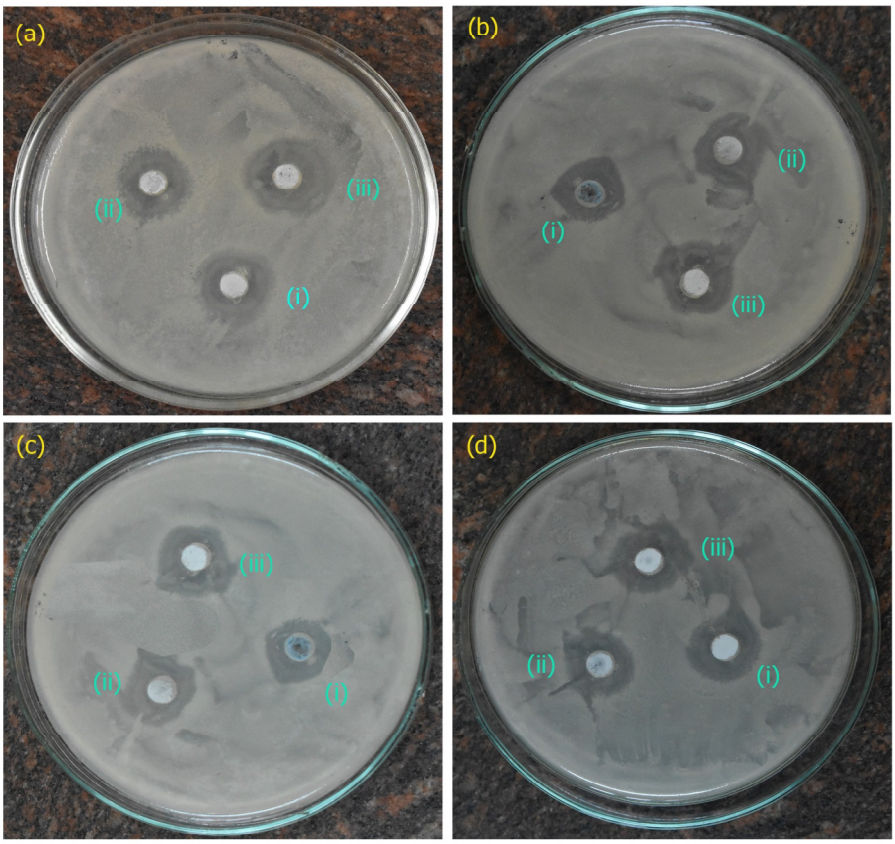

Fig. 8. The antibacterial activity of the samples derived from natural source against E. coli (a) and S. aureus (b), and chemical source against E. coli (c) and S. aureus (d). In every plate, samples such as HAp, HAp/PEG and HAp/PVP are represented by (i), (ii) and (iii), respectively.

[DOI: 10.22068/ijmse.18.1.10]

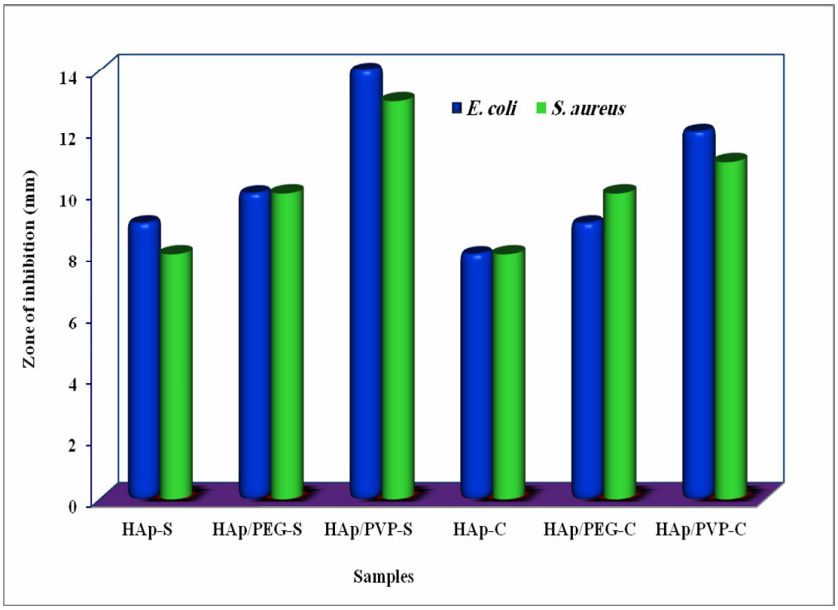

Fig. 9. Zone of inhibition (mm) of the samples derived from both sources against E. coli and S. aureus.

3.6. Comparative Analysis

Based on the essential properties such as high carbonate presence, less crystalline nature, low crystallite size, suitable mechanical property, rod like morphology and high antibacterial effect for bio-medical applications, HAp/PVP derived from both sources are taken for comparative analysis on the basis of obtained functional, structural, chemical, morphological and biological characteristics and comparative results are as follows.

On the basis of functional group and phases:

- In both sources, characteristics peaks of PO_4^{3-}, OH^- and CO_3^{2-} are presented with a change in intensities, and typical characteristics peaks of HAp are observed with a change in intensities and broadness (hexagonal phase (JCPDS: 09-0432)).

On the basis of crystalline nature:

- The formation of well crystalline nature of the product could be assessed by the presence of triplet (632, 601 and 572 cm^{-1}). The intensity of the triplet is high in the HAp/PVP-C and it is not visible (changed into doublet) in the HAp/PVP-S. Thus, HAp/PVP-S has a relatively less crystalline nature (Figure 10) due to the high substitution of CO_3^{2-} and the presence of sodium [57]. This less crystalline nature is also assessed by the Crystallinity Index calculation and broadness of the XRD characteristics peaks.

On the basis of structural properties:

- The growth of 'c' axis could be assessed by increasing the intensity of (002) as observed in HAp/PVP-S which indicates the formation of rod like structure [45] in the product that favors for bone related applications.
- The crystallite size of HAp/PVP-S is low (Figure 10) which is assessed by peak broadening and Debye's-Scherrer formula. Reduced crystallite size finds many applications as already discussed.
- The decrease in lattice constant 'a' and increase in 'c' value are observed in both products, which also favor for the rod like morphology [13].
- The HAp/PVP-S has good mechanical property (Figure 10) for bio-medical applications.

On the basis of Elemental (Chemical) compositions:

- Interestingly, additional favorable elements such C and Na with Ca, P and O are presented in HAp/PVP-S (Figure 10). Sudip Mondal et al. [6], Giraldo-Betancur et al. [1] and Sassa et al.[17] have derived HAp from natural tuna fish, bovine and pig bone respectively, and observed the same presence of elements in HAp lattice.
- The Ca/P ratio of HAp/PVP-S is high and more deviated from the theoretical ratio due to the presence of additional elements. It was achieved in the non-stoichiometric HAp

[DOI: 10.22068/ijmse.18.1.10]

derived from different natural sources include fish bone [6], bovine bone [1, 18], pig bones [17], mammalian and marine sources, egg shell and mussel shell [11].

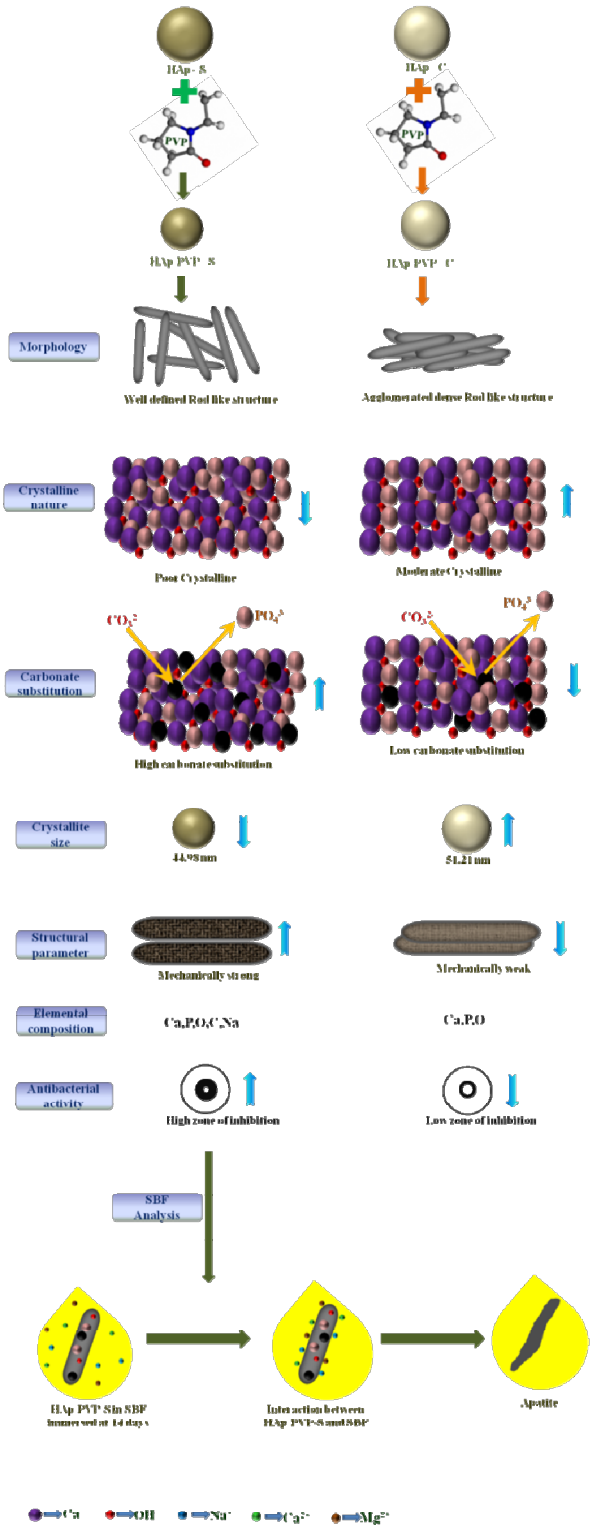

Fig. 10. Comparative results between HAp/PVP-S and HAp-PVP-C, and formation mechanism of apatite.

[DOI: 10.22068/ijmse.18.1.10]

On the basis of the morphology of the products:

- Both products exhibit rod like morphology. HAp/PVP-S shows the well defined rod like whereas HAp/PVP-C shows agglomerated dense rod like with improper structure (Figure 10). Among the various morphology, rod like shapes are highly preferred for various applications include constructing the microstructure of teeth [45], bone tissue engineering [57, 58], drug delivery systems [58] and other biomedical applications [57].

On the basis of antibacterial activity:

- HAp/PVP-S has good sensible antibacterial activity against the E. coli and S. aureus due to the high zones of inhibition than HAp/PVP-C (Figure 10). As HAp/PVP-S has low crystalline nature, it has a better rate of dissolution and antibacterial activity, as indicated by the larger zone of inhibition [59]. Due to the high negativity in HAp/PVP-S (more carbonate substitutions), more ion exchange can be possible which may lead to loss of cell membrane integrity, DNA rupture and ultimately death of cells (appeared as the zone of inhibition) [56].

On the basis of the amount of carbonate:

- The relatively high amount of carbonate B can be assessed in the HAp/PVP-S (Figure 10) by the presence of intense carbonate peaks at 1460, 1412 and 875 cm^{-1}, increases in the c-axis, decreases in the a-axis, increases in c/a value, reduced crystallite size and nature, percentage of carbon through EDX analysis, high C/P ratio, deviation in Ca/P ratio and high zone of inhibition. A comparative study has been carried out effectively between the natural and chemical sources by Sossa et al. [17], Giraldo-Betancur et al. [1] and Rahavi et al. [15], they got the same result (presence of high amount of carbonate B in the naturally derived HAp). They strongly pointed out that this presence favors the bioactivity of HAp powders and assists to bone tissue growth for osteoblast proliferation when implant, loading and releasing drugs as already discussed.

As characteristics of HAp/PVP-S include high carbonate presence, low crystallite size, poor crystalline nature, presence of trace metal, non-stoichiometric elemental composition and rod like crystals with several nanometers in thickness and tens of nanometers in length are matched with the characteristics of biological apatite, it is important to ensure the apatite formation ability of HAp/PVP-S by SBF analysis.

3.7. SBF Analysis

Figure 11 (a, b and c) shows the surface morphology of the HAp/PVP-S after being soaked in the SBF for various days such as 3, 7 and 14 days, respectively at 37 ± 0.5ºC. Though the apatite formation is taking place for the surface of all the HAp/PVP-S (3, 7 and 14 days), the amount of apatite formed and the surface coverage varied specifically. The surface is not completely covered with apatite growth after 3 days (Figure 11a) of immersion, after 7 days, irregular apatite growth is formed (Figure 11b) and finally after 14 days (Figure 11c), the surface of HAp/PVP-S is completely covered by more apatite growth. The formation of pores and dense apatite layer is noticed in HAp/PVP-S nanoparticles. These formations in the apatite structure can improve the osteoconduction and osteointegration properties [60]. Hence, apatite forming ability is favorable for HAp/PVP-S at 14 days of immersion in SBF solution.

The apatite formation process mainly depends on the negative group, which depends on a large number of negative ions (PO_4^{3-} and OH^-) on the surface [17]. The positive ions include Ca^{2+}, Mg^{2+}, Na^{2+} from SBF are attracted by the PO_4^{3-} ions present on the surface of the sample during the soaking period (Figure 10). The apatite crystal is formed due to the ion exchange between HAp/PVP-S and SBF [17]. More number of CO_3^{2-} (negative charge carriers) substitution in HAp/PVP-S structure supports the formation of apatite [17]. Thus, the surface of HAp/PVP-S has negatively charged OH^- and PO_4^{3-} ions which attract the positively charged ions present in the surrounding SBF. Most of the nanoparticles were joined together (having large surface energy) to form agglomerated apatite.

[DOI: 10.22068/ijmse.18.1.10]

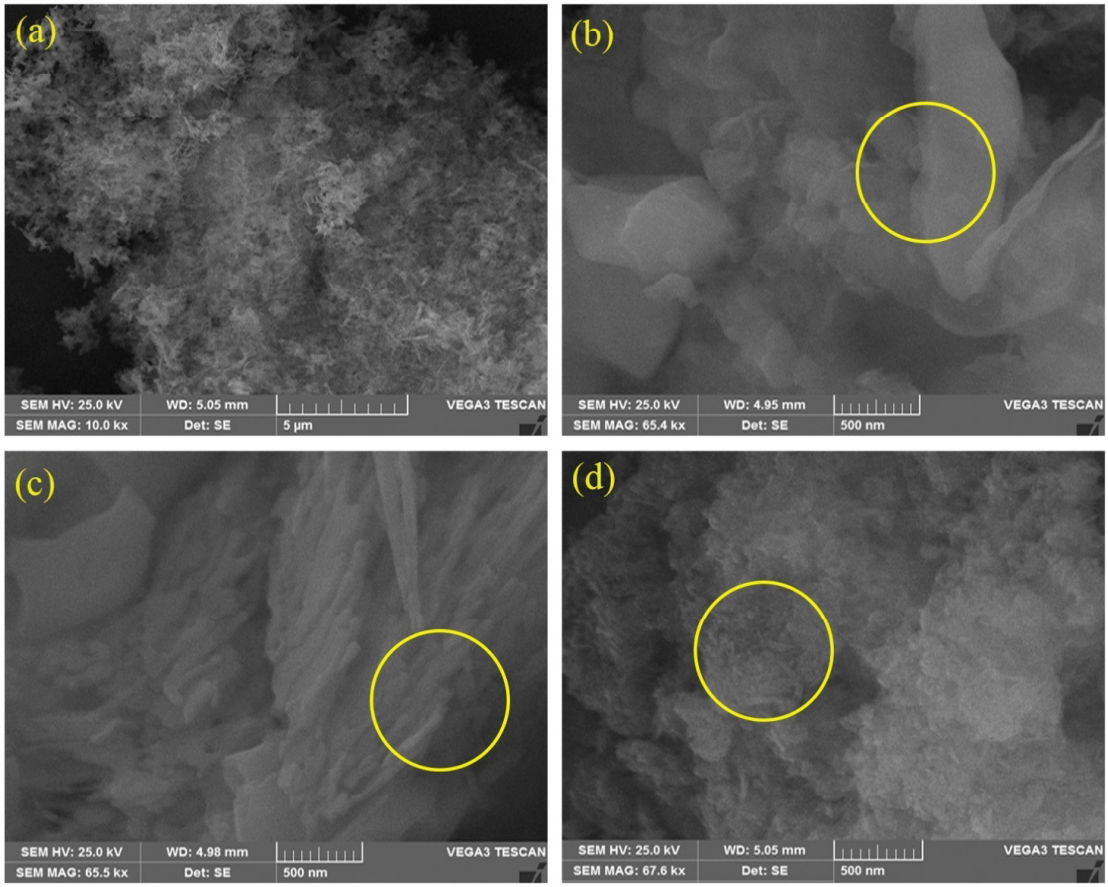

Fig. 11. Surface morphology of the HAp/PVP-S nanorods without soaking in SBF (a), soaked for 3 (b), 7 (c) and 14 (d) days. Note: The apatite layer can be seen in the circled spots.

4. CONCLUSION

Hydroxyapatite (HAp), HAp/PEG and HAp/PVP have been prepared from both Gastropod shell (natural source) and chemical source by precipitation method, and are characterized and compared. Formations of HAp in chemically derived products and from Gastropod shell are assessed by the presence of functional groups and characteristics planes of XRD. The amount of carbonate content, crystalline nature and structural characteristics are assessed for all the products. HAp/PVP-S exhibits high carbonate content, reduction of crystallite size and crystalline nature and favorable mechanical property. Both SEM and TEM analyses exhibit useful rod like morphology in HAp/PVP derived from both sources due to the hydrogen bond formed between PVP and HAp, also Ostwald ripening and Oriented attachment. The antibacterial activities of the products show that considerable activity exists in all the products, due to the high negativity in HAp/PVP and low crystallite size, HAp/PVP-S has high antibacterial activity. Comparative analysis shows that HAp/PVP-S has high carbonate content, low crystallite size, poor crystalline nature, the presence of trace metal elements, non-stoichiometric composition, rod- like crystals, good antibacterial activity and apatite forming ability at after 14 days of immersion. As these properties are matched with the characteristics of biological apatite in human, HAp/PVP-S may be suitable for forming bone apatite. Transformation of the sea shell waste into valuable HAp can be considered to be an environmentally friendly, sustainable and economical process since these shells are available in large quantities.

[DOI: 10.22068/ijmse.18.1.10]

REFERENCES

1. Giraldo-Betancur, A.L., Epinosa-Arbelaez, D.G., Real-Lopez, A.D. and Millan-Malo, B.M., "Comparison of physicochemical properties of bio and commercial Hydroxyapatite." Curr. Appl. Phys., 2013, 13, 1383 – 1390.
2. Vijayalakshmi, V., Mayya, V., Keerthiga, V. and Shinde, V., "Comparative studies of hydroxyapatite (HAp) nanoparticles synthesized by using different green templates" AIP Conf. Proc., 2020, 080002-1–080002-11.
3. Markovi, S., Veselinovi, L., Luki, M. J., Karanovi, L., Cko, I. B., Ignjatovi, N. and Uskokovi, D., "Synthetical bone-like and biological hydroxyapatites: A comparative study of crystal structure and morphology." Biomed. Mater., 2011, 6, 045005-045018.
4. Ou-Yang, H., Paschalis, E. P., Mayo, W. E., Boskey, A. L. and Mendelsohn, R., "Infrared Microscopic Imaging of Bone: Spatial Distribution of CO_3^{2-}." J. Bone Miner. Res., 2001, 16, 893-900.
5. Muhammad Syazwan, M. N. and Yanny Marliana, B. I., "The in□uence of simultaneous divalent cations (Mg^{2+}, Co^{2+} and Sr^{2+}) substitution on the physico-chemical properties of carbonated Hydroxyapatite." Ceram. Int., 2019, 45, 14783-14788.
6. Mondal, S., Hoang, G., Manivasagan, P., Moorthy, M. S., Kim, H. H., Vy Phan, T. T. and Oh, J., "Comparative characterization of biogenic and chemical synthesized Hydroxyapatite biomaterials for potential biomedical application." Mater. Chem. Phys., 2019, 228, 344-356.
7. Başargan, T., Erdol-Aydin, N. and Nasun-Saygili G., "In situ Biomimetic Synthesis to Produce Hydroxyapatite – Polyvinyl Alcohol Biocomposites: Precipitation and Spray Drying Methods." Polym. Plast. Technol. Eng., 2016, 55, 447-452.
8. Barabas, R., Melinda, C., Imre, D., Liliana, B. and Erzsebet, S.B., "Comparative study of particle size analysis of hydroxyapatite-based nanomaterials." Chem. Pap., 2013, 67, 1414-1423.
9. Zhang, H., Liu, M., Fan, H. and Zhang, X., "Carbonated Nano Hydroxyapatite Crystal Growth Modulated by Poly(ethylene glycol) with Different Molecular Weights." Cryst. Growth Des., 2012, 12, 2204−2212.
10. Hayashi, K., Kishida, R., Tsuchiya, A. and Ishikawa, K., "Honeycomb blocks composed of carbonate apatite, β-tricalcium phosphate, and hydroxyapatite for bone regeneration: effects of composition on biological responses." Mater. Today Bio., 2019, 4, 100031.
11. Mohd Pu'ad, N. A. S., Koshy, P., Abdullah, H. Z., Idris, M. I. and Lee, T. C., "Syntheses of hydroxyapatite from natural sources." Heliyon, 2019, 5, e01588.
12. Londono-Restrepo, S. M., Zubieta-Otero, L. F., Jeronimo-Cruz, R., Mondragon, M. A. and Rodriguez-García, M. E., "Effect of the Crystal Size on the infrared and Raman Spectra of bio hydroxyapatite of human, bovine, and porcine bones." J. Raman Spectrosc., 2019, 50, 1120-1129.
13. Murugan, R. and Ramakrishna, S., "Crystallographic Study of Hydroxyapatite Bioceramics Derived from Various Sources." Cryst. Growth Des., 2005, 5, 111-112.
14. Swain, S. K. and Sarkar, D., "A comparative study: Hydroxyapatite spherical nanopowders and elongated nanorods." Ceram. Int., 2011, 37, 2927-2930.
15. Rahavi, S. S., Ghaderi, O., Monshi, A. and Fathi, M. H., "A comparative study on physicochemical properties of hydroxyapatite powders derived from natural and synthetic sources." Russ. J. Non-ferrous Metals, 2017, 58, 276-286.
16. Ramesh, S., Natasha, A. N., Tan, C. Y., Bang, L. T., Niakan, A., Purbolaksono, J., Chandran, H., Ching, C. Y., Ramesh, S. and Teng, W. D., "Characteristics and properties of hydoxyapatite derived by sol–gel and wet chemical precipitation methods." Ceram. Int., 2015, 41, 10434-10441.
17. Sossa, P. A. F., Giraldo, B. S., Garcia, B. C. G., Parra, E. R. and Arango, P. J. A., "Comparative study between natural and synthetic Hydroxyapatite: structural, morphological and bioactivity properties." Revista Materia., 2018, 23, e-12217.
18. Yelten, A. and Yilmaz, S., "Comparison of Naturally and Synthetically Derived Hydroxyapatite Powders." Acta Phys. Pol. A., 2017, 131, 55-58.

[DOI: 10.22068/ijmse.18.1.10]

19. Pal, A., Maity, S., Chabri, S., Bera, S., Chowdhury, A.R., Das, M. and Sinha, A., "Mechanochemical synthesis of nanocrystalline hydroxyapatite from Mercenaria clam shells and phosphoric acid." Biomed. Phys. Eng. Express, 2017, 3, 015010.
20. Lee, S-W., Balázsi, C., Balázsi, K., Seo, D., Kim, H.S., Kim, C-H. and Kim, S-G., "Comparative Study of hydroxyapatite prepared from seashells and eggshells as a bone graft material." Tissue Eng. Regen. Med., 2014, 11, 113-120.
21. Othman, R., Mustafa, Z., Loon, C.W. and Noor, A.F.M., "Effect of calcium precursors and pH on the precipitation of carbonated Hydroxyapatite." Procedia. Chem., 2016, 19, 539–545.
22. Dhanaraj, K. and Suresh, G., "Conversion of waste sea shell (Anadara granosa) into valuable nanohydroxyapatite (nHAp) for biomedical applications." Vacuum, 2018, 152, 222–230.
23. Morris, J. P., Wang, Y., Backeljau, T. and Chapelle, G., "Biomimetic and bio-inspired uses of mollusc shells." Mar. Genomics, 2016, 27, 85-90.
24. Tank, K. P., Chudasama, K. S., Thaker, V. S. and Joshi, M. J., "Pure and zinc doped nano-hydroxyapatite: Synthesis, characterization, antimicrobial and hemolytic studies." J. Cryst. Growth, 2014, 401, 474–479.
25. Lala, S., Ghosh, M., Das, P. K., Das, D., Kar, T. and Pradhan, S. K., "Magnesium substitution in carbonated hydroxyapatite: Structural and microstructural characterization by Rietveld's refinement." Mater. Chem. Phys., 2016, 170, 319-329.
26. Youness, R. A., Taha, M. A., Elhaes, H. and Ibrahim, M., "Molecular Modeling, FTIR Spectral Characterization and Mechanical Properties of Carbonated-Hydroxyapatite Prepared by Mechanochemical Synthesis." Mater. Chem. Phys., 2017, 190, 209-218.
27. Youness, R. A., Taha, M. A. and Ibrahim, M.A., "Effect of sintering temperatures on the in vitro bioactivity, molecular structure and mechanical properties of titanium / carbonated Hydroxyapatite nanobiocomposites." J. Mol. Struct., 2017, 1150, 188-195.
28. Tkalcec, E., Popovic, J., Orlic, S., Milardovic, S. and Ivankovic, H., "Hydrothermal synthesis and thermal evolution of carbonate-fluorhydroxyapatite scaffold from cuttle fish bones." Mater. Sci. Eng. C., 2014, 42, 578–586.
29. Rey, C., Collins, B., Goehl, T., Dickson, I.R. and Glimcher, M. J., "The Carbonate Environment in Bone Mineral: A Resolution-Enhanced Fourier Transform Infrared Spectroscopy Study." Calcif. Tissue Int., 1989, 45, 157-164.
30. Ren, F., Ding, Y. and Leng Y., "Infrared spectroscopic characterization of carbonated apatite:A combined experimental and computational study." J. Biomed. Mater. Res A., 2013, 102, 496–505.
31. Bang, L. T., Long, B. D. and Othman, R., "Carbonate Hydroxyapatite and Silicon-Substituted Carbonate Hydroxyapatite: Synthesis, Mechanical Properties, and Solubility Evaluations." Sci.World J., 2014, 969876, 1-9.
32. Kuriakose, T. A., Kalkura, S. N., Palanichamy, M., Arivuoli, D., Dierks, K., Bocelli, G. and Betzel, C., "Synthesis of stoichiometric nano crystalline hydroxyapatite by ethanol-based sol–gel technique at low temperature." J. cryst. Growth, 2004, 263, 517-523.
33. Thirugnanam, T., "Effect of Polymers (PEG and PVP) on Sol-Gel Synthesis of Microsized Zinc Oxide." J. Nanomater., 2013, 362175, 1-7.
34. Lopes C de, C. A., Limirio, P. H. J. O., Novais, V. R. and Dechichi, P., "Fourier transform infrared spectroscopy (FTIR) application chemical characterization of enamel, dentin and bone." Appl. Spectrosc. Rev., 2018, 53, 747-769.
35. Nagy, G., Lorand, T., Patonai, Z., Montsko, G., Bajnoczky, I., Marcsik, A. and Mark, L., "Analysis of pathological and non-pathological human skeletal remains by FT-IR spectroscopy." Forensic Sci. Int., 2008, 175, 55-60.
36. Eyes-Gasga, J., Martínez-Piñeiro, E. L., Rodríguez-Álvarez, G., Tiznado-Orozco, G.E., García-García, R. and Brès, E.F., "XRD and FTIR crystallinity indices in sound human tooth enamel and synthetic Hydroxyapatite." Mater. Sci. Eng C., 2013, 33, 4568-4574.

[DOI: 10.22068/ijmse.18.1.10]

37. Sa, Y., Guo, Y., Feng, X., Wang, M., Li, P., Gao, Y., Yang, X. and Jiang, T., "Are different crystallinity-index-calculating methods of hydroxyapatite efficient and consistent?." New J. Chem., 2017, 41, 5723-5731.
38. Shemesh, A., "Crystallinity and diagenesis of sedimentary apatite." Geochim. Cosmochim. Acta., 1990, 54, 2433-2438.
39. Person, A., Bocherens, H., Jean-François Saliege, Paris, F., Zeitoun, V. and Gerard, M., "Early Diagenetic Evolution of Bone Phosphate: An X-ray Diffractometry Analysis." J. Archaeol. Sci., 1995, 22, 211-221.
40. Suresh Kumar, C., Dhanaraj, K., Vimalathithan, R.M., Ilaiyaraja, P. and Suresh, G., "Hydroxyapatite for bone related applications derived from sea shell waste by simple precipitation method." J. Asian Ceram. Soc., 2020, 8, 416-429.
41. Wright, L. E. and Schwarcz, H. P., "Infrared and Isotopic Evidence for Diagenesis of Bone Apatite at Dos Pilas, Guatemala: Palaeodietary Implications." J. Archaeol. Sci., 1996, 23, 933-944.
42. Riaz, M., Zia, R., Ijaz, A., Hussain, T., Mohsin, M. and Malik A., "Synthesis of monophasic Ag doped hydroxyapatite and evaluation of antibacterial activity." Mater. Sci. Eng C., 2018, 90, 308–313.
43. Qian, G., Liu, W., Zheng, L. and Liu, L., "Facile synthesis of three dimensional porous hydroxyapatite using carboxymethylcellulose as a template." Results Phys., 2017, 7, 1623–1627.
44. Mishra, V. K., Bhattacharjee, B. N., Parkash, O., Kumar, D. and Rai, S. B., "Mg-doped hydroxyapatite nanoplates for biomedical applications: A surfactant assisted microwave synthesis and spectroscopic investigations." J. Alloys Compd., 2014, 614, 283-288.
45. Klinkaewnarong, J. and Utara, S., "Ultrasonic-assisted conversion of limestone into needle-like hydroxyapatite nanoparticles." Ultrason. Sonochem., 2018, 46, 18-25.
46. Ramasamy, V., Anand, P. and Suresh, G., "Synthesis and characterization of polymer-mediated $CaCO_3$ nanoparticles using limestone: A novel approach." Adv. Powder Technol., 2018, 29, 818–834.
47. Landi, E., Celotti, G., Logroscino, G. and Tampieri A., "Carbonated hydroxyapatite as bone substitute." J. Eur. Ceram. Soc., 2003, 23, 2931–2937.
48. Shanmugam, N., Dhanaraj, K., Viruthagiri, G., Balamurugan, K. and Deivam, K., "Synthesis and characterization of surfactant assisted Mn^{2+} doped ZnO nanocrystals." Arab. J. Chem., 2016, 9, S758–S764.
49. Ramasamy, V. and Vijayalakshmi, G., "Effect of Zn doping on structural optical and thermal propertice of CeO_2 nanoparticles." Superlattices microstruct., 2015, 85, 510-515.
50. Shi, X., Li, M., Yang, H., Chen, S., Yuan, L., Zhang, K. and Sun, J., "PEG-300 assisted hydrothermal synthesis of $4ZnO.B_2O_3.H_2O$ nanorods." Mater. Res. Bull., 2007, 42, 1649-1656.
51. Parra, M. R. and Haque, F. Z., "Poly (Ethylene Glycol) (PEG)-assisted shape-controlled synthesis of one-dimensional ZnO nanorods." Optik, 2015, 126, 1562-1566.
52. Nathanael, A. J., Seo, Y. H. and Oh, T. H., "PVP Assisted Synthesis of Hydroxyapatite Nanorods with Tunable Aspect Ratio and Bioactivity." J. Nanomater., 2015, 621785, 1-9.
53. Zhang, Y. and Lu, J., "A Mild and Ef□cient Biomimetic Synthesis of Rodlike Hydroxyapatite Particles with a High Aspect Ratio Using Polyvinylpyrrolidone As Capping Agent." Cryst. Growth Des., 2008, 8, 2101-2107.
54. Nathanael, A. J., Han, S. S. and Oh T. H., "Polymer-Assisted Hydrothermal Synthesis of Hierarchically Arranged Hydroxyapatite Nanoceramic." J. Nanomater., 2013, 962026, 1-8.
55. De Maeyer, E. A. P., Verbeeck, R. M. H. and Pieters, I. Y., "Effect of K^+ on the Stoichiometry of Carbonated Hydroxyapatite Obtained by the Hydrolysis of Monetite." Inorg. Chem., 1996, 35, 857-863.
56. Mehta, P. and Kaith, B.S., "In-situ fabrication of rod shaped nano-hydroxyapatite using microwave assisted semi-interpenetrating network as a template-morphology controlled approach." Mater. Chem. Phy., 2018, 208, 49-60.

[DOI: 10.22068/ijmse.18.1.10]

57. K-hasuwan, P., Kuanchertchoo, N., Wetprasit, N. and Supaphol, P., "Hydroxyapatite/ovalbumin composite particles as model protein carriers for bone tissue engineering: I. Synthesis and characterization." Mater. Sci. Eng C., 2012, 32, 758–762.
58. Bricha, M., Belmamouni, Y., Essassi, E. M., Ferreira, J. M. F. and Mabrouk, K. E., "Surfactant-Assisted Hydrothermal Synthesis of Hydroxyapatite Nanopowders." J. Nanosci. Nanotechnol., 2012, 12, 8042-8049.
59. Jadalannagari, S., Deshmukh, K., Ramanan, S. R. and Kowshik, M., "Antimicrobial activity of hemocompatible silver doped hydroxyapatite nanoparticles synthesized by modi□ed sol–gel technique." Appl. Nanosci., 2014, 4, 133-141.
60. Gopi, D., Ramya, S., Rajeswari, D., Karthikeyan, P. and Kavitha, L., "Strontium, cerium co-substituted hydroxyapatite nanoparticles: Synthesis, characterization, antibacterial activity towards prokaryotic strains and in vitro studies." Colloids and Surf. A: Physicochem. Eng. Aspects, 2014, 451, 172–180.

[DOI: 10.22068/ijmse.18.1.10]